Constraining aerosol optical models using ground-based, collocated particle size and mass measurements in variable air mass regimes during the 7-SEAS/Dongsha Experiment

Shaun W. Bell[a,b] Richard A. Hansell[c,b], Judith C. Chow[d], Si-Chee Tsay[b,*], Sheng-Hsiang Wang[e,c,b], Qiang Ji[c,b], Can Li[c,b], John G. Watson[d], and Andrey Khlystov[f]

[a] Science Systems and Applications Inc., Lanham, Maryland, USA
[b] Goddard Space Flight Center, NASA, Greenbelt, Maryland, USA
[c] Earth System Science Interdisciplinary Center, University of Maryland, College Park, Maryland, USA
[d] Division of Atmospheric Sciences, Desert Research Institute, Reno, Nevada, USA
[e] Department of Atmospheric Sciences, National Central University, Jhongli, Taiwan
[f] Department of Civil and Environmental Engineering, Duke University, Durham, NC,USA

To be submitted to *Atmospheric Environment* Special Issue on

Observation, Modeling and Impact Studies of Biomass Burning and Pollution in the SE Asian Environment

January 25, 2012

*Corresponding author
Tel./Fax: +1-301-614-6188
E-mail address: Richard.A.Hansell@nasa.gov

Abstract

During the spring of 2010, NASA Goddard's COMMIT ground-based mobile laboratory was stationed on Dongsha Island off the southwest coast of Taiwan, in preparation for the upcoming 2012 7-SEAS field campaign. The measurement period offered a unique opportunity for conducting detailed investigations of the optical properties of aerosols associated with different air mass regimes including background maritime and those contaminated by anthropogenic air pollution and mineral dust. What appears to be the first time for this region, a shortwave optical closure experiment for both scattering and absorption was attempted over a 12-day period during which aerosols exhibited the most change. Constraints to the optical model included combined SMPS and APS number concentration data for a continuum of fine and coarse-mode particle sizes up to $PM_{2.5}$. We also take advantage of an IMPROVE chemical sampler to help constrain aerosol composition and mass partitioning of key elemental species including sea-salt, particulate organic matter, soil, non sea-salt sulphate, nitrate, and elemental carbon. Our results demonstrate that the observed aerosol scattering and absorption for these diverse air masses are reasonably captured by the model, where peak aerosol events and transitions between key aerosols types are evident. Signatures of heavy polluted aerosol composed mostly of ammonium and non sea-salt sulphate mixed with some dust with transitions to background sea-salt conditions are apparent in the absorption data, which is particularly reassuring owing to the large variability in the imaginary component of the refractive indices. Extinctive features at significantly smaller time scales than the one-day sample period of IMPROVE are more difficult to reproduce, as this requires further knowledge concerning the source apportionment of major chemical components in the model. Consistency between the measured and modeled optical parameters serves as an important link for advancing remote sensing and climate research studies in dynamic aerosol-rich environments like Dongsha.

1. Introduction

It is well known that aerosols and their optical properties of scattering and absorption play a considerable role in climate forcing and as such have a large impact on public policy (Forster et al., 2007). The radiative effects of aerosols have been a primary focus of numerous research studies over the past decade, particularly as advances in aerosol optical modeling (e.g., Nousiainen et al. 2009) and the rapid growths in field and laboratory measurements (e.g., Reid et al. 2008; Volten et al. 2001) have significantly improved our understanding of the role of aerosols on our environment. The challenges in elucidating these radiative effects lie in the complex spatial and temporal interplay of the aerosol's physicochemical properties with the ambient electromagnetic fields along with changes in the thermodynamic state of the atmosphere. These challenges become even more daunting when aerosols from disparate air mass regimes converge making it exceedingly difficult to separate the extinctive properties and radiative contributions of the component aerosol species.

The fundamental question we seek to answer in this study is how well one can capture the observed optical properties of aerosols in model simulations using simple parameterizations constrained by ground-based measurements. Moreover, how well can these properties be captured in a dynamic atmospheric environment where the air masses and aerosols are constantly changing? To address this question we take advantage of the extended suite of aerosol instrumentation found in NASA Goddard's Chemical, Optical, Microphysical Measurements of In-situ Troposphere (COMMIT) ground-based mobile laboratory (http://smartlabs.gsfc.nasa.gov/) which was deployed at Dongsha Island in the northern South China Sea (SCS) during the spring of 2010 in support of the 7-SEAS field experiment and inter-comparison study (Lin et al. 2012 - this issue and the references therein). Further discussions of

88 instrumentation, site topology, and scientific background for the investigation can be found in
89 Wang et al. (2011) as well as other studies in this special issue. For brevity, the primary
90 instruments and resulting datasets employed in this study are given in Table 1 followed by more
91 detailed descriptions in section 2. Additional information can also be found in various other
92 literature including Li et al. (2012 - this issue) and (2010), Jeong et al. (2008), and at the above
93 web link.

94 Because of the annual climate of the northern SCS and its tendency to be shaped by changes
95 in the Asian monsoonal winds, Dongsha is ideally suited for this study. Prevailing southwesterly
96 and northeasterly flows during the months of June-September and November-April, respectively
97 can lead to high aerosol loading events stemming from a variety of sources including urban
98 pollution, biomass burning smoke, wind-blown desert dust, and sea-salt over much of the Asian
99 continent (Tsay et al. 2009) and surrounding coastal regions. Consequently the northern SCS is at
100 a confluence of many different aerosols and thus lends a perfect opportunity for not only testing
101 the self-consistency of our ground-based measurements but also attempting optical closure which
102 is crucial for remote sensing and climate studies.

103 For years, the aerosol community has been actively engaged in the age old, ill-posed
104 problem of bridging together the modeling and observational perspectives of an aerosol's optical
105 properties. The degree of closure is a function of many parameters including how well the
106 measurements are known (i.e. the uncertainty) of the aerosol property being investigated and
107 how well the model is constrained using independent observations. Many past studies have
108 focused exclusively on the light scattering properties of aerosols (e.g., Cai et al. 2011)
109 particularly in regions concerned about air quality and visibility reduction (e.g., Cabada et al.
110 2004). Others have examined aerosol extinctive properties from specific aerosol events such as

111 those due to biomass burning activities (e.g., Reid et al. 2005; Mack et al. 2010; Malm et al.
112 2005) and those derived from urban and industrialized sources (e.g., Highwood et al. 2011; Ma et
113 al. 2011). Lack of key measurements has also required that some studies make assumptions
114 regarding the aerosols' properties, such as for example, chemical composition (e.g., Lee, 2009).
115 To the best of our knowledge, detailed closure studies of scattering and absorption have not yet
116 been conducted at Dongsha in the northern SCS. This recent deployment offers a unique
117 opportunity for using an extensive measurement set to probe the optical properties of multiple
118 aerosol types. This was the primary impetus for the current study given the availability of
119 measurements and diversity of aerosols encountered during the 7SEAS/Dongsha Experiment.

120 During the deployment (March – May 2010), an extended array of *in-situ* measurements
121 characterized the physicochemical properties of aerosols. This study focuses on a twelve day
122 window from 25 March - 27 April 2010 during which different aerosols were observed using an
123 IMPROVE (A modified Interagency Monitoring of PROtected Visual Environments) chemical
124 sampler. These days were chosen to maximize the different aerosol types analyzed. Continuous
125 sampling revealed a number of key chemical species associated with anthropogenic air pollution,
126 mineral dust, and sea-salt. Atwood et al. (2012 - this issue) also observed similar aerosol
127 components at Dongsha using a collocated 8-stage drum impactor. Back trajectory and
128 subsequent cluster analysis from Wang et al. (2012 - this issue) lend support to the origins of the
129 different air masses and aerosols and their respective transport paths during the experiment. This
130 is later addressed in section 3. To exploit the particle size information of our measurements,
131 SMPS and APS number concentration data are combined for a continuous distribution of both
132 fine and coarse-mode particle sizes up to $PM_{2.5.}$ Estimated total mass from the particle size
133 measurements is then compared to that from a collocated TEOM for validation purposes.

Furthermore, IMPROVE data along with some assumptions regarding source apportionment, was utilized as a supplementary constraint to help facilitate distributing aerosol mass in the light-scattering model simulations. Lastly, model comparisons with both light scattering (nephelometer) and absorption (PSAP) measurements were assessed to gauge the overall convergence of the shortwave (SW) optical parameters. This is important for two main reasons: (1) to provide a firm anchor point for remote sensing and radiative studies during 7-SEAS and beyond and (2) to later extend the SW optical properties for which most ambient aerosols are measured, into the longer wavelengths to help probe the thermal emissions of the atmosphere (e.g., Hansell et al. 2011).

Despite the advantages of having an extended instrument suite, there are still inherent complexities and uncertainties in characterizing the physicochemical properties of aerosols, particularly for multiple aerosol systems. This includes such unknowns as particle morphology, aerosol mixing state, surface roughness, etc. In addition to the fundamental limitations in measurements and techniques, including temporal and spatial resolution of the instruments, the current study relies on a number of basic assumptions which are listed in Table 2 along with their supporting rationale.

The paper is arranged as follows: Description of instrumentation, data analysis, light scattering model and methodology are presented in section 2; aerosol chemistry and particle size results along with comparisons of the measured and modeled extinctive parameters and their implications are examined in section 3, and finally a summary and future works are discussed in section 4.

2. Instrumentation/Data Analysis, Model Overview, and Methodology

a. *IMPROVE Chemical Sampler*

A modified IMPROVE sampler with an Air Industrial Hygiene Laboratory (AIHL) 2.5 μm-cut cyclone, operated at 22.8 L/min flow rate was used for sampling. As shown in Figure 1, sampling was conducted on three parallel channels equipped with 25 mm Teflon®-membrane (R2PI025; Teflo® PTET membrane with polymethyl propylene support; 2 μm pore size), quartz-fiber (TissuQuartz 2500 QAT-UP), and nylon-membrane (1.0 μm pore size, all filters from Pall Life Sciences, Ann Arbor, MI) filters at a flow rate of 6 L/min per channel (leaving 4.8 L/min on the bypass channel). Details of the IMPROVE chemical analysis performed at the Desert Research Institute (DRI) are given below.

Unexposed filters are subject to pre-treatment, followed by acceptance testing to ensure there is no contamination prior to the measurement process. Teflon-membrane filters are equilibrated in a constant temperature (25 ± 1.5 °C) and relative humidity (35 ± 5%) environment for a minimum of 48 hours before weighing. Gravimetric analysis is performed using a microbalance (Mettler MT-5, Hightown, NJ) with a sensitivity of ±1 μg. Quartz-fiber filters are pre-fired at 900 °C for four hours to remove organic artifact, sealed, and stored under refrigeration prior to field sampling. Nylon-membrane filters in 47 mm diameter discs are punched to accommodate a 25 mm sampling cassette.

Analysis of 51 elements (Na to U) was conducted by X-ray fluorescence (XRF) spectrometry (PanAlytical Epsilon 5, Almelo, the Netherlands) on Teflon-membrane filters using 13 secondary targets (Watson et al., 1999). Nylon-membrane filters were extracted in 15 ml of distilled-deionized water (DDW) with one hour each sonication and mechanical shaking. Extracts are stored under refrigeration overnight before being submitted for anion analyses of

chloride (Cl^-), nitrate (NO_3^-), and sulfate ($SO_4^{=}$) by ion chromatography (IC; Dionex ICS-3000, Sunnyvale, CA; Chow and Watson, 1999); cation analysis of water-soluble ammonium (NH_4^+) by automated colorimetry (AC; Astoria 302A Colorimetry System, Astoria, OR), and water-soluble sodium (Na^+) and potassium (K^+) by atomic absorption spectrometry (AAS; Varian Spectro800, Walnut Creek, CA).

A 0.5 cm^2 punch of quartz-fiber filter was submitted for organic and elemental carbon (OC and EC, respectively), and thermal carbon fractions (OC1–OC4 at 140, 280, 480, and 580 °C in a 100% helium [He] atmosphere and EC1–EC3 at 580, 780, and 880 °C in a 98% He/2% oxygen [O_2] atmosphere, respectively. Pyrolyzed OC [i.e., OP] is determined based on laser reflectance) following the IMPROVE_A protocol (Chow et al., 2007; 2011) using the DRI Model 2001 thermal/optical carbon analyzer (Atmoslytic, Calabasas, CA). This standard protocol for OC (sum of OC1+OC2+OC3+OC4+OP) and EC (sum of EC1+EC2+EC3-OP) has been applied in the U.S. long-term non-urban IMPROVE network and the urban Chemical Speciation Network. A minimum of 10% of the samples are submitted for replicate analyses following the quality assurance/quality control (QA/QC) procedure specified in Chow and Watson (2012). The reported concentration in $\mu g/m^3$ is blank subtracted and error propagated following the procedure described in Bevington (1969).

b. ***Combined APS-SMPS Aerosol Size Distributions***

Combining data from multiple aerosol-sizing instruments is desirable in order to obtain the largest possible continuum of particle sizing information, however, most instruments measure different approximations of particle size (mobility, aerodynamic, and geometric). The TSI SMPS measures particle mobility size and is used for submicron particles whereas the TSI APS

measures aerodynamic size and measures predominantly super micron particles. These differences must be accounted for when combining the size distributions from these instruments. Khlystov et al. (2004) present an innovative approach to combine the mobility distribution from the SMPS with the aerodynamic distribution from the APS via a statistical approach that requires no a-priori information regarding particle density (ρ) or shape.

Converting number concentrations to equivalent surface and volume distributions is straight forward as it only implies assumptions regarding particle shape. For simplicity, all particles in this study are considered spherical although it is recognized that the shapes of aerosol particles vary widely and can include highly irregular non-symmetric particles as in the case of dust. Converting to mass distributions can be a bit more cumbersome as it involves estimates of both particle density and shape factor (χ). Additionally, many of these instruments have engineering limitations when trying to measure denser aspherical particles, which convolute the resulting size distributions even further. For brevity, the largest and most important assumptions are stated below; however the reader is referred to Khlystov et al. (2004) for more detail.

Although the APS and SMPS use fundamentally different approaches, both instruments attempt to characterize the number concentration at discrete size intervals. The aerodynamic diameter measured and reported by the APS is predominantly a function of particle asphericity and density, whereas the mobility diameter measured and reported by the SMPS is a function of asphericity but not density. An in-depth review of the varying terminologies and definitions for conversion between various definitions of diameter can be found in Decarlo et al. (2004). First, we assume the instrument counting efficiency to be unity in the overlapping regions between the two instruments (540-800nm) and second, the SMPS log-weighted number concentration profile for the overlapping region is approximated by a log-linear fit. This smoothes the SMPS profile

for the APS fitting. The log-weighted number concentration of the APS is then shifted along the diameter axis until, via a minimized error approach following equation 1 in Khlystov et al. (2004), it matches with the log-linear fit to the SMPS. The amount the APS is shifted is proportional to the square root of the particle density in the instrument overlap region and the asphericity of the particles. The size correction factor for converting aerodynamic to electro-mobility diameter [Khlystov et al. (2004)] is defined as:

$$\alpha = \sqrt{\frac{\rho_p}{\chi \rho_0}}$$

where ρ_p is the particle density, ρ_0 is the reference density of 1 g cm^{-3}, and χ is the shape factor. Under a spherical assumption, we can then retrieve a rough bulk density approximation from the APS correction (Khlystov et al. 2004 - valid only in the overlap region, but used for the entire size distribution in our study) which is discussed later in section 3. For this study, the APS and SMPS size spectra are taken during 18 second and 3 minute sample periods, respectively. The resulting distributions are then averaged into 2-hour bins yielding ~360 and 40 samples, respectively.

c. *Light-Scattering Model and Methodology*

Assuming that the aerosols are spherical, we employ the Lorenz-Mie light-scattering code (Mishchenko et al. 1998) to calculate the extinction cross sections used for the bulk extinction parameters from each of the chemical compositions and mixtures at a wavelength of λ=550nm. We choose λ=550nm since we can apply the nephelometer (Anderson and Ogren, 1998) and PSAP (Bond et al. 1999) corrections for later comparison of the measurements and model data.

All Mie code computations are performed over the range of particle sizes measured by the combined APS-SMPS instruments for each chemical component. Following (Petty, 2004), the bulk volume extinction coefficients β_e of scattering (β_s) and absorption (β_a) are given by:

$$\beta_e = \sum_i \sum_j N_{i,j} \sigma_{e\,i,j}$$

where $\boldsymbol{\sigma_e}$ is the Mie calculated extinction cross section and N is the number concentration from the particle size instruments. Here we assume a homogenous mixture of pure aerosol types (i), i.e., no coatings or inclusions are considered for simplicity, over a range of particle diameters (j).

A summary of the methodology employed in this study is given in Figure 2. We first start with the data from the IMPROVE sampler as our basis for determining the content and distribution of aerosol particulates representing the different air mass regimes encountered during the study. After combining the number concentration profiles which span the particle size range of 10nm to 2.5μm, we partition the IMPROVE data as a function of size. The mass distributions of the combined profiles are then weighted by uniformly adjusting all size bins by the estimated mass fractions from IMPROVE. Next, we take the weighted chemical speciated mass profiles and calculate the implied number distributions using the assumed bulk densities given in Table 3. After running the Mie code, we integrate the size dependent Mie solutions over the number size distributions for each chemical constituent from ~10nm (bottom end of the SMPS) to 2.5μm. Note that fine particles were expected at Dongsha and therefore all *in-situ* extinction instruments had a sharp cyclone size cut of ~2.5μm which was the upper end of our particle sampling size. The integrated results yield rough bulk scattering and absorption coefficients for each of the chemical species, which are linearly combined to give the total optical parameters to be compared with the measurements. Optical consistency in this regard lends credence to the

chemical partitioning and composition assumptions used, which will allow us to further hypothesize about applying this methodology for future inter-comparisons with LW measurements such as those from SMART's AERI interferometer (e.g., Hansell et al. 2008).

3. Results and Discussion

Here we examine the resulting IMPROVE chemical data and combined APS-SMPS particle size measurements which are used to constrain the light scattering model. The derived model parameters are then compared with those from measurements in order to gauge the optical consistency.

a. *Aerosol Chemistry*

After the chemical analysis, the basic elements where characterized using the mass conversion factors from IMPROVE (Watson, 2002) and Sillanpää (2006) to determine rough allotments of bulk chemical constituent properties. The resulting primary elements are listed in Table 3 along with their appropriate data conversions, corresponding refractive indices at λ=550nm, and other relevant parameters. These data are used to reconstruct the total mass to compared mass by gravimetry and to provide rough allocations of particulate constituent in order to constrain the optical calculations. The resulting mass fractions of the key chemical species for the period analyzed are shown in Figure 3. The reconstructions account for ~75% of the total weight of the filter depending on the sample. Total mass differences can likely be attributed to several things including (1) unused trace chemical species, (2) measurement uncertainties, and (3) differences in mass conversion factors employed. The latter point is clearly illustrated with sea salt. For example, using Sillanpää (2006), the mass fraction of sea salt can be up to 50%

295 larger than that obtained following IMPROVE's methodology, which consequently increases the
296 reconstructed mass anywhere between 80-100% of the total $PM_{2.5}$ weighed mass. For sea salt, we
297 apply the conversion factors from IMPROVE (Table 3).

298 For the most part, NSS and sea salt, likely stemming from transport over
299 urban/industrialized regions along the coast, dominate the mass distributions both by quantity
300 and by mass fraction. This finding is corroborated by Wang et al. (2012 - this issue) whose study
301 shows that the majority of air mass transport (~52%) into Dongsha follows two primary paths:
302 one that originates from the inland areas of northern China and Mongolia and then travels
303 towards the coast and a second that originates along the coastal regions of China. Because the
304 coast is known to have higher anthropogenic emissions (Streets et al., 2003), the transported air
305 masses into Dongsha will contain a larger number of industrialized pollutants as reflected in
306 Figure 3. Since Dongsha is an atoll, the sea salt distribution is not surprising and likely represents
307 background aerosol conditions for the region. Other dominant classifications evident from the
308 analysis are ammonium and nitrate which in the form of ammonium nitrate accounts for about
309 9.7±2.3% of the measured $PM_{2.5}$. Various trace chemical constituents such as As, Cd, Co, Cr,
310 etc, were also identified and used in the reconstruction (labeled as 'other elements' in Figure 3 to
311 maintain consistency with Sillanpää [2006]). Since the combined mass fraction of these trace
312 species is small relative to the other components, these were not considered in the study.

313 Soil particles (e.g., mineral dust) likely transported from northern China and Mongolia
314 (e.g., Taklimakan and Gobi deserts) were also identified, however, their mass fractions over the
315 12-day period were generally less than those found for NSS and sea salt. It is noted that a major
316 dust event which affected a large area including Dongsha had occurred just days before the

317 IMPROVE sampler began recording data (~21 March 2010). Observation and modeling
318 perspectives of this event can be found in Wang et al. (2011) and Bian et al. (2011), respectively.
319
320 **b.** ***Merged particle size spectra and estimated density***
321 Figures 4(a) and 4(b) provide examples of the fitting process and final outcome for 26
322 March, and the mean fit for 27-29 March, respectively. The aforementioned fitting is done on
323 two-hour averaged particle size data from the SMPS and APS instruments which provide us a
324 time series of estimated size correction factors, and therefore estimated particle densities which
325 were found to mostly vary between ~1.2-2.2 g/cm^3 (Figure 4c). Note that estimated densities on
326 the lower end of the range reflect higher relative humidity values while those values that are
327 much less than one are due to instrumental effects. To simplify the conversion from number
328 concentration profiles to mass concentration profiles for the modeling portion of our study, an
329 average of the "correction factor" derived density is used which was found to be ~1.76 g/cm^3.
330 This is consistent with aerosol that is mostly dominated by NSS (Table 3) however; the range
331 also overlaps with the densities for sea salt and various minerals found in soil aerosol. Although
332 spherical assumptions required for merging the particle size spectra could result in overestimated
333 density values, there is reasonable agreement between the retrieved integrated mass
334 concentrations from the size fitting process and collocated TEOM measurements (Figure 5).
335 Here we use the $PM_{2.5}$ TEOM from the Taiwan Environmental Protection Administration (T-
336 EPA, http://www.epa.gov.tw/en/) mobile facility for comparison. It is evident that the retrieved
337 mass is somewhat larger than the TEOM values, which could be due to the spherical assumptions
338 used. This offset could also be due to the TEOM losing volatiles (e.g., ammonium nitrate and
339 some organic matter) and/or residual water inside the SMPS/APS. The corresponding linear

correlation coefficient is ~0.70 and the resulting fitting parameters are 0.94 (slope) and 7.3 (offset). It is also noted that the total mass computed from the IMPROVE data compared to within about 10% of the TEOM values (not shown).

c. ***Comparison of optical parameters***

The comparisons between modeled and measured optical parameters are presented in Figure 6, where panels (a-b) and (c-d) show the time series and scatter plots for both absorption and scattering coefficients, respectively. Included on the scatter plots are error bars associated with the measurement uncertainties which are taken to be about 15% and 25% for the nephelometer (Anderson et al. 1996) and PSAP (Bond et al. 1999), respectively. Uncertainties in the model parameters are estimated to be on the order of ~30% based on previous works (e.g., Ma et al. 2011). The linear correlation coefficients for scattering and absorption were 0.47 and 0.56, respectively. On close inspection of Figures 6(b)-6(d), it is apparent that scattering was over predicted (> 3σ standard deviations) on 26 March likely due to changes in our constant relative mass fractions assumption for the chemical constituents. After removing this point, the linear correlation coefficient for scattering increased to 0.84. The smaller correlation for absorption is not surprising since the imaginary term of the refractive index for these aerosols varies by orders of magnitude (Table 3), which in turn can lead to a much larger variability in the absorption coefficient. Linear fits to the scattering and absorption data (red lines shown in Figure 6) reveal fitting parameters of 0.35 (slope) and 29.61 (intercept) and 0.43 (slope) and 3.0 (intercept), respectively. The large intercepts are related to model uncertainties. If the offsets are forced through zero (i.e., model uncertainties are reduced), the resulting slopes for scattering and absorption are 0.67 and 0.75, respectively.

Given the assumptions (Table 2), the observations were reasonably tracked by the model, although in terms of absolute differences, scattering is continuously underestimated [Figure 6(d)] particularly when the measurements are greater than ~50Mm^{-1}. A plausible reason for this disparity is hydroscopic growth on the particles during periods of higher relative humidity which leads to an increase in scattering. This is related to the study's dry particle assumptions where periods with lower relative humidity are expected to converge more closely to the measured results. Modeled absorption values on the other agreed surprisingly well with the measurements up to ~10Mm^{-1}; however for higher measured absorption the model data exhibited greater scatter.

Excluding absolute differences, the model peaks in scattering and absorption are nearly consistent with those from measurements. This is particularly apparent during late March and early April, where absorption underwent a series of rapid changes likely related to the differences found in mass fractions of the component aerosols [Figure 3(a)]. The IMPROVE data between 26-31 March for example, show some of the highest recorded levels of pollution (NSS) and soil aerosols during the study period. This is consistent with the analysis from Wang et al. (2012 - this issue) showing high-level transport of air masses from dust source regions in China influenced by urban and industrialized sources along the coast. Higher levels of sulphates mixed with transported and localized sea salt, would help explain the periods when absorption was minimal, for example on 26 March, where transported air masses mostly originated from the coastal regions of China. Following this event, the total aerosol mass decreased by almost 40% so the effects of carbonaceous particles became more prominent leading to a period of higher absorption around 27-28 March. The overestimated absorption as shown is potentially due to the excess soot in the model or it could be due to equally applying the aerosol mass across all particle size bins. Later in March sea salt aerosols become more predominate, coinciding with

386 the region's background maritime conditions and the absorption begins to fall off again.

387 It is immediately apparent that for a dynamic aerosol rich environment like Dongsha, one
388 cannot simply prescribe *a priori* an assumed aerosol composition of one type which could cause
389 large errors in the modeled parameters. This is particularly more evident for absorption than it is
390 for scattering since the real part of the refractive index only varies by ~30% over the species
391 analyzed, whereas absorption can vary by several orders of magnitude. Assuming sea salt to be
392 the dominant aerosol for example, will largely underestimate total absorption which
393 consequently will impact studies of radiative transfer. Unless aerosol measurements are made at
394 or near their sources, it is essential to adequately account for any changes in the aerosol's
395 composition. It is further noted that additional knowledge concerning the source apportionment
396 of major chemical components relative to particle size should help improve the model's
397 performance. Instead of uniformly scaling all size bins of the SMPS-APS spectra by an aerosol's
398 mass fractional data, only the size bins appropriate to the species under investigation should be
399 scaled.

400

401 **4. Conclusions and Future Work**

402 The aim of this study was to not only test the self-consistency of NASA Goddard's
403 COMMIT ground-based measurements but was also to attempt optical closure for the first time
404 in the dynamic aerosol-rich environment at Dongsha Island off the southwest coast of Taiwan
405 during the 7-SEAS/Dongsha experiment (2010). Comprehensive aerosol physicochemical
406 measurements were used for constraining the optical model to compare derived extinctive
407 parameters with those that were measured. Critical to this study was the use of an IMPROVE

sampler to enhance our knowledge of the aerosol's changing chemical composition. Given the assumptions required to partition the chemical and microphysical data, the model is able to reasonably track the observations and identify peak events in both scattering and absorption over a 12-day test period. Transitions in key aerosol types from heavy polluted aerosol composed mostly of ammonium and NSS mixed with some dust to mainly sea salt are evident in the absorption data, which is particularly reassuring owing to the large variability in the imaginary component of the refractive indices. Overall, scattering is shown to be negatively biased because of the dry particle assumptions employed in the study, whereas the modeled absorption agrees reasonably well with the measurements. Uniform scaling of the particle size spectra by an aerosol's mass fractional data may have also contributed to the model's bias.

Instrumental limitations such as not being able to account for the role of water vapor on particle growth rates along with uncertainties in the measurements and the techniques employed, makes it difficult to achieve full optical closure (complete alignment along the 1:1 line) in a region that is characterized by a diversity of air mass regimes and aerosols. However, given the limitations and uncertainties in this study, the amount of closure or optical consistency attained, is encouraging as measured by the ability to adequately reproduce the observed behavior in the extinctive parameters. To improve the convergence of the model data with the measurements will require additional key information including:

- Further knowledge concerning the source apportionment of major chemical components in the optical model at higher temporal resolution for capturing the daily evolution of an aerosol's composition.
- The requirement to only scale the particle size bins appropriate to the chemical species under investigation.
- Selecting appropriate optical constants for the chemical species identified
- Consideration to the aspherical nature of aerosol particles and the use of numerical light scattering codes for handling these more complex geometries.
- Extending measurement capabilities to account for the effects of relative humidity on

particle growth rates and its impact on merging the particle size spectra.

Regarding the final point, the relative humidity issues experienced at Dongsha adds substantially to the error in the APS-SMPS size distribution merger. A combination of hydrophobic and hydrophyillic particles skews the bulk density towards that of pure water. However, particle growth due to increased humidity is difficult to parameterize from our existing instrument setup. Current modifications to the COMMIT mobile facility are underway to eliminate the inadvertent role of moisture (by drying out the aerosol stream prior to evaluation) or to quantify the relative growth rates of particles (via tandem DMA's, CCN counters, and wet/dry nephelometry). Furthermore extinction instruments which are not biased by relative humidity or varying corrections due to multiple scattering, such as the Aethelometer and PSAP, are also being integrated into the facility.

This study illustrates the significance of employing a synergy of multiple ground-based measurements for characterizing the physicochemical properties of multiple aerosols in an optical model for closure experiments involving both scattering and absorption. It represents a first step at attempting closure for the dynamic aerosol-rich environment at Dongsha. With further instrument modifications and the application of new techniques, it is anticipated that improved closure can be obtained which will certainly benefit remote sensing and climate studies in this important region.

Acknowledgements

This work was supported by the NASA Radiation Sciences Program managed by Dr. Hal B. Maring. We are grateful to Taiwan's Environmental Protection Administration for providing the necessary logistical support during the deployment of NASA's COMMIT laboratory at Dongsha. We would like to thank Dr. Chuck McDade of the University of California, Davis, for providing 50 IMPROVE cassettes, and Mr. Steve Kohl of DRI's Environmental Analysis Facility for coordinating field operation and conducting chemical analyses and data validation. Lastly, we express thanks to Dr. Mishchenko for making his Lorenz- Mie light scattering code available for public use.

478 References
479
480 Anderson, T. L., and J. A. Ogren (1998), Determining aerosol radiative properties using the TSI 3563
481 Integrating Nephelometer, Aerosol Sci. Technol., 29, 57–69, doi:10.1080/02786829808965551.
482
483 Atwood, S., J.S. Reid, S.M. Kreidenweis, S. Cliff, Y. Zhao, N.-H. Lin, and D.L. Westphal (2012), Size
484 Resolved Measurements of Springtime Aerosol Particles over the Northern South China Sea: Source
485 identification, *Atmos. Environ.* for special issue.
486
487 Bevington, P.R. (1969). *Data Reduction and Error Analysis for the Physical Sciences*. McGraw Hill:
488 New York, NY.

489 Bian, H., X. Tie, J. Cao, Z. Ying, S. Han, and Y. Xue (2011), Analysis of a Severe Dust Storm Event over
490 China: Application of the WRF-Dust Model, *Aerosol and Air Quality Research*, **11**: 419-428.

491 Bond, T.C., T.L. Anderson, and D. Campbell (1999), Calibration and intercomparison of filter-based
492 measurements of visible light absorption by aerosols. *Aerosol Science and Technology*, **30**(6): 582-
493 600.
494
495 Cabada, J. C., A. Khlystov, A. E. Wittig, C. Pilinis, and S. N. Pandis (2004), Light scattering by fine
496 particles during the Pittsburgh Air Quality Study: Measurements and modeling, *J. Geophys. Res.*,
497 **109**, D16S03, doi:10.1029/2003JD004155.
498
499 Cai, Y., D. C. Montague, and T. Deshler (2011), Comparison of measured and calculated scattering from
500 surface aerosols with an average, a size-dependent, and a time-dependent refractive index, *J.*
501 *Geophys. Res.*, **116**, D02202, doi:10.1029/2010JD014607.
502
503 Chow, J.C., and J.G. Watson (1999), Ion chromatography in elemental analysis of airborne particles. In
504 *Elemental Analysis of Airborne Particles, Vol. 1*, Landsberger, S., Creatchman, M., Eds.; Gordon and
505 Breach Science: Amsterdam, 97-137.

506 Chow, J.C., J.G.Watson, L.-W.A. Chen, M.C.O. Chang, N.F. Robinson, D.L. Trimble, S.D. Kohl
507 (2007), The IMPROVE_A temperature protocol for thermal/optical carbon analysis: Maintaining
508 consistency with a long-term database. *J. Air Waste Manage. Assoc.*, **57**(9):1014-1023.
509 http://pubs.awma.org/gsearch/journal/2007/9/10.3155-1047-3289.57.9.1014.pdf.

510 Chow, J.C., J.G. Watson, J. Robles, X.L. Wang, L.-W.A. Chen, D.L. Trimble, S.D. Kohl, R.J. Tropp,
511 K.K. Fung (2011) Quality assurance and quality control for thermal/optical analysis of aerosol
512 samples for organic and elemental carbon. *Anal. Bioanal. Chem.*, **401**(10):online. DOI
513 10.1007/s00216-011-5103-3. http://www.springerlink.com/content/a60122x13p757421/fulltext.pdf.

514 Chow, J.C. and J.G. Watson (2012). Aerosol chemical analysis on filters. In *Aerosols Handbook :*
515 *Measurement, Dosimetry, and Health Effects*, 2; Ruzer, L., Harley, N. H., Eds.; CRC Press/Taylor &
516 Francis: New York, NY, accepted.

517 DeCarlo, P.F., J. G. Slowik, D. R. Worsnop, P. Davidovits, and J.L. Jimenez (2004), Particle Morphology
518 and Density Characterization by Combined Mobility and Aerodynamic Diameter Measurements:
519 Part 1: Theory, *Aerosol Sci. and Technol.* **38**:1185-1205.
520

Forster, P., and Coauthors (2007), Changes in atmospheric constituents and in radiative forcing. Climate Change 2007: The Physical Science Basis. S. Solomon et al., Eds., Cambridge University Press, 129–234.

Gysel, M., M. Laborde, J.S. Olfert, R. Subramanian, and A.J. Gröhn 2011, Effective density of Aquadag and fullerene soot black carbon reference materials used for SP2 calibration, *Atmos. Meas. Tech*., **4**, 2851–2858, doi:10.5194/amt-4-2851-2011

Hansell, R. A., K. N. Liou, S. C. Ou, S. C. Tsay, Q. Ji, and J. S. Reid (2008), Remote Sensing of Mineral Dust Aerosol using AERI during the UAE2: A Modeling and Sensitivity Study, *J. Geophys. Res.*, **113**, D18202, doi: 10.1029/2008JD010246.

Hansell, R. A., J. S. Reid, S. C. Tsay, T. L. Roush, and O. V. Kalashnikova (2011), A Sensitivity Study on the Effects of Particle Chemistry, Asphericity and Size on the Mass Extinction Efficiency of Mineral Dust in the Earth's Atmosphere: From the Near to Thermal IR, *Atmos. Chem. Phys*., **11**, 1527–1547, doi:10.5194/acp-11-1527-2011.

Highwood, E.J., M.J. Northway, G.R. McMeeking, W.T. Morgan, D. Liu, S. Osborne, K. Bower, H. Coe, C. Ryder, and P. Williams (2011), Scattering and absorption by aerosols during EUCAARI-LONGREX: can airborne measurements and models agree?, *Atmos. Chem. Phys. Discuss.,* **11**, 18487–18525, doi:10.5194/acp-11-18487-2011.

Jeong, M.-J., S.-C. Tsay, Q. Ji, N. C. Hsu, R. A. Hansell, and J. Lee (2008), Ground-based measurements of airborne Saharan dust in marine environment during the NAMMA field experiment, *Geophys. Res. Lett.*, **35**, L20805, doi:10.1029/2008GL035587

Kalashnikova, O. V. and I.N. Sokolik (2002), Importance of shapes and compositions of wind-blown dust particles for remote sensing at solar wavelengths, *Geophys. Res. Lett*., **29** (10), 1398, doi: 10.1029/2002GL014947.

Kandler, K., N. Benker, U. Bundke, E. Cuevas, M. Ebert, P. Knippertz, S. Rodríguez, L. Schütz, S. Weinbruch, chemical composition and complex refractive index of Saharan Mineral Dust at Izaña, Tenerife (Spain) derived by electron microscopy, *Atmos. Environ.* **41**, 8058–8074.

Khlystov, A., C. Stanier, and S.N. Pandis (2004), An algorithm for combining electrical mobility and aerodynamic size distributions data when measuring ambient aerosol. *Aerosol Sci. and Technol.* **38**:229-238.

Lee, Y. 2009, In situ Measurements of Asian Dust Aerosols off the California Coast: Optical Closure, *Asia-Pacific J. Atmos. Sci.*, **45**, 293-305

Li, C., S.-C. Tsay, N. C. Hsu, J. Y. Kim, S. G. Howell, B. J. Huebert, Q. Ji, M.J. Jeong, S.-H. Wang, R.A.Hansell, and S.W. Bell (2012), Characteristics and Composition of Atmospheric Aerosols in Phimai, Central Thailand during BASE-ASIA, *Atmos. Environ.* for special issue.

Li, C., S.-C. Tsay, J.S. Fu, R.R. Dickerson, Q. Ji, S.W. Bell, Y. Gao, W. Zhang, J. Huang, Z. Li, and H. Chen (2010), Anthropogenic air pollution observed near dust source regions in northwestern China during springtime 2008, *J. Geophys. Res*., **115**, D00K22, doi: 10.1029/ 2009JD013659.

570 Lin, N.-H., S.-C. Tsay, J.S. Reid, H.B. Maring, B.N. Holben, N.C. Hsu, S.-H. Wang (2012), Overview of
571 regional experiments on biomass burning aerosols and related pollutants in Southeast Asia, *Atmos.*
572 *Environ.* for special issue.
573
574 Lloyd, J.A., K.J. Heaton, and M.V. Johnston (2009), Reactive Uptake of Trimethylamine into
575 Ammonium Nitrate Particles, *J. Phys. Chem. A*., **113** (17), 4840-4843, doi: 10.1021/jp900634d.
576
577 Ma N., C.S. Zhao, A. Nowak, T. Müller, S. Pfeifer, Y.F. Cheng, Z.Z. Deng, P.F. Liu, W.Y. Xu, L. Ran, P.
578 Yan, T. Göbel, E. Hallbauer, K. Mildenberger, S. Henning, J. Yu, L.L. Chen, X.J. Zhou, F.
579 Stratmann, and A. Wiedensohler (2011), Aerosol optical properties in the North China Plain during
580 HaChi campaign: an in-situ optical closure study, *Atmos. Chem. Phys*., **11**, 5959–5973,
581 doi:10.5194/acp-11-5959-2011.
582
583 Mack, L.A., E. J. T. Levin, S. M. Kreidenweis, D. Obrist, H. Moosmüller, K. A. Lewis, W. P. Arnott,
584 G. R. McMeeking, A. P. Sullivan, C. E. Wold, W.-M. Hao, J. L. Collett Jr., and W. C. Malm (2010),
585 Optical closure experiments for biomass smoke aerosols, *Atmos. Chem. Phys.*, **10**, 9017-9026
586
587 Malm, W. C., D. E. Day, C. Carrico, S. M. Kreidenweis, J. L. Collett Jr., G. McMeeking, T. Lee, J.
588 Carrillo, and B. Schichtel (2005), Intercomparison and closure calculations using measurements of
589 aerosol species and optical properties during the Yosemite Aerosol Characterization Study, *J.*
590 *Geophys. Res.*, **110**, D14302, doi:10.1029/2004JD005494.
591
592 Mishchenko, M. I., A. A. Lacis, B. E. Carlson, and L. D. Travis (1995), Nonsphericity of Dust-like
593 Tropospheric Aerosols: Implications for Aerosol Remote Sensing and Climate Modeling, *Geophys.*
594 *Res. Lett.,* **22,** 1077–1080.
595
596 Nousiainen, T. (2009), Optical Modeling of Mineral Dust Particles: A Review, *J. Quant. Spectrosc.*
597 *Radiat. Transfer***, 110**, 1261-1279.
598
599 Patterson, E. M. (1981), Optical properties of the crustal aerosol: Relation to chemical and physical
600 characteristics, *J. Geophys. Res*., **86,** 3236-3246
601
602 Petty, G. W. (2004), A First Course in Atmospheric Radiation, Sundog Publishing, Madison WI, pp 445
603
604 Reid, J.S., T.F. Eck, S.A. Christopher, R. Koppmann, O. Dubovik, D.P. Eleuterio, B.N. Holben, E.A.
605 Reid, and J. Zhang (2005), A review of biomass burning emissions part III: intensive optical
606 properties of biomass burning particles, *Atmos. Chem. Phys*., **5**, 827–849.
607
608 Reid, J.S., E. A. Reid, A. Walker, S. Piketh, S. Cliff, A. Al Mandoos,S.-C. Tsay, and T. F. Eck (2008),
609 Dynamics of southwest Asian dust particle size characteristics with implications for global dust
610 research. *J. Geophys. Res*., **113**, D14212, doi:10.1029/ 2007JD009752.
611
612 Schkolnik, G., D. Chand, A. Hoffer, M.O. Andreae, C. Erlick, E. Swietlicki, Y. Rudich (2007),
613 Constraining the density and complex refractive index of elemental and organic carbon in biomass
614 burning aerosol using optical and chemical measurements, *Atmos. Environ.* **41**, 1107–1118.
615
616 Shettle, E. P., and R. W. Fenn (1979), Models for the Aerosols for the Lower Atmosphere and the Effects
617 of Humidity Variations on Their Optical Properties, *AFGL-TR-79-0214 Environmental Research,*
618 Paper 676.

619 Sillanpää, M.,R. Hillamo, S. Saarikoski, A. Frey, A. Pennanen, U. Makkonen, Z. Spolnik, R. V. Grieken,

M. Branis, B. Brunekreef, M.-C. Chalbot, T. Kuhlbusch, J. Sunyer, V.-M. Kerminen, M. Kulmala, and R. O. Salonen (2006), Chemical composition and mass closure of particulate material at six urban sites in Europe. *Atmos. Environ.* **40**, S212–S223.

Streets D.G., T.C. Bond, G.R. Carmichael, S.D. Fernandes, Q. Fu, D. He, Z. Klimont, S.M. Nelson, N.Y. Tsai, M.Q. Wang, J.-H. Woo, K.F. Yarber (2003), An inventory of gaseous and primary aerosol emissions in Asia in the year 2000, *J. Geophys. Res*., **108**, 8809, doi:10.1029/ 2002JD003093..

Toon, O.B., J.B. Pollack, and B.N. Khare (1976), The optical constants of several atmospheric aerosol species ammonium sulfate, aluminum oxide, and sodium chloride, *J. Geophys. Res*., **81,** 5733-5748

Turpin B.J. and H.-J Lim (2001), Species contributions to $PM_{2.5}$ mass concentrations: Revisiting common assumptions for estimating organic mass, Aerosol Science and Technology, 35, 602-610.

Tsay, S.-C. (2009), Outbreaks of Asian Dust Storms: An Overview from Satellite and Surface Perspectives, *Recent Progress in Atmospheric Sciences: Applications to the Asia Pacific Region*, K. N. Liou and M. D. Chou, (Eds.), *World Scientific Publishing*, 373-401.

Volten, H., O. Muñoz, E. Rol, J. F. de Haan, W. Vassen, J. W. Hovenier, K. Muinonen, and T. Nousiainen (2001), Scattering matrices of mineral aerosol particles at 441.6 nm and 632.8 nm, *J. Geophys. Res.*, **106**, 17,375–17,401, doi:10.1029/2001JD900068.

Wang, S-H., S.-C. Tsay, N.-H. Lin, N.C. Hsu, S.W. Bell, C. Li, Q. Ji, M.J. Jeong, R. A. Hansell, E.J. Welton, B.N. Holben, G.-R. Sheu, Y.-C. Chu, S.-C. Chang, J.-J. Liu, and W.-L. Chiang (2011), First detailed observations of long-range transported dust over the northern South China Sea, *Atmos. Environ.* **45**, 4804–4808.

Wang, S-H., S.-C. Tsay, N.-H. Lin, S.-C. Chang, C. Li, E.J. Welton, B.N. Holben, K.M. Lau,C.-C. Kuo, H.-P. Chia, C.-Y. Chiu, S.W. Bell, Q. Ji, R.A. Hansell, and C.-M. Peng (2012), Characteristics of the origin, transport, and vertical distribution of atmospheric pollutants during 7SEAS/Dongsha experiment, *Atmos. Environ.* for special issue.

Watson, J.G., J.C. Chow, C.A. Frazier (1999), X-ray fluorescence analysis of ambient air samples. In *Elemental Analysis of Airborne Particles, Vol. 1*, Landsberger, S., Creatchman, M., Eds.; Gordon and Breach Science: Amsterdam, 67-96.

Watson, J.G. (2002), Visibility: Science and Regulation, *Air & Waste Manage. Assoc.* **52**: 628-713

669 **Table 1 Primary Instrument at COMMIT and Data**

Instrument	Data
IMPROVE chemical sampler[(1)]	Chemical composition and mass partitioning of aerosols
APS (TSI 3321)[(2)]	Coarse-mode particle size distributions
SMPS (TSI)[(3)]	Fine-mode particle size distributions
3 Wavelength PSAP (Radiance Research, Inc.)[(4)]	Aerosol absorption coefficients
3 Wavelength Nephelometer (TSI)[(5)]	Aerosol scattering coefficients
TEOM (model 1400ab; R&P Co.)[(6)]	Mass concentrations

670 [(1)] Interagency Monitoring of PROtected Visual Environments
671 [(2)] Aerodynamical Particle Sizer
672 [(3)] Scanning Mobility Particle Sizer
673 [(4)] Particle/Soot Absorption Photometer (@0.55μm corrected for sample spot size and flow rate)
674 [(5)] Nephelometer @0.55μm with Anderson corrections applied
675 [(6)] Tapered Element Oscillating Microbalance;
676 Note- for additional comparisons, we used the TEOM from the Taiwan Environmental Protection
677 Administration mobile facility.

678

679

680

681

682

683

684

685

686

687

688

689

690

Table 2 Key Assumptions in Study
1. Although aerosol particles are rarely spherical in shape, we assume for simplicity that all particles are spheres and apply the Lorenz-Mie light scattering code (Mishchenko et al. 1995) for calculating the scattering and absorption coefficients. The optical parameters for non-spherical distributions of dust particles, for example, are generally larger than those for spheres (e.g., Kalashnikova et al. 2002 and Hansell et al. 2011) however, this should not impact the ability of the model to track the measurements.
2. Assuming spheres, particle density is inferred from combining SMPS-APS particle size spectra following Khlystov et al. (2004). Although spherical assumptions could result in overestimated density values, SMPS-APS mass measurements show good agreement with those from a collocated TEOM suggesting this is a reasonable assumption.
3. All optical constants used to characterize the elemental species identified by IMPROVE are based on data availability and the representativeness of the data to the measurements. Table 3 identifies the datasets used in the study.
4. For simplicity, all particles are considered to be dry in this experiment, although relative humidity was high at Dongsha. Aerosols with absorbed water exhibit larger β_{ext} due to the larger optical cross sections. Lack of hydroscopic growth on particles could underestimate β_{ext}. However, the ability to track the measurements should not be impacted. Improved convergence is expected to occur for lower relative humidity cases.
5. Fine particles were expected at Dongsha and therefore all optical instruments had a sharp cyclone size cut of ~2.5μm. To maintain consistency, a numerical size cut on the combined size distribution of $PM_{2.5}$ was made.
6. All aerosol components are uniformly weighted by the calculated IMPROVE mass fraction (i.e., no assumptions are made to preferentially bin certain species such as dust being greater than 0.5μm).
7. IMPROVE data were averaged (obtained) over 24-hour sampling periods. As long as the relative mass fractions of multiple chemical constituents remains constant, this will not impact the findings significantly; however, large differences in mass fraction (e.g., significant changes in air mass during a sample) will invalidate this assumption.

691

692

693

694

695

Figure 1 Modified Interagency Monitoring of PROtected Visual Environments (IMPROVE) sampler including Air Industrial Hygiene Laboratory (AIHL) 2.5 µm-cut cyclone.

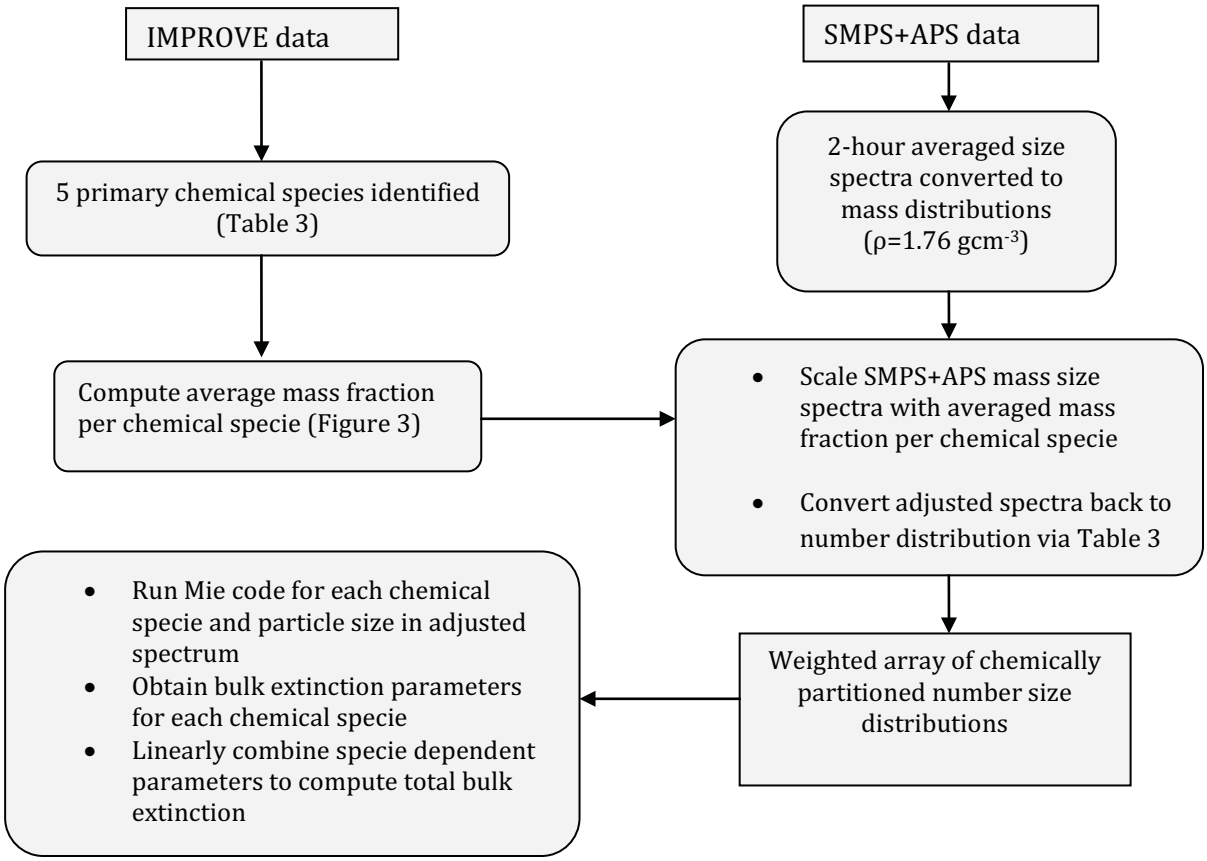

Figure 2 Flow diagram depicting methodology

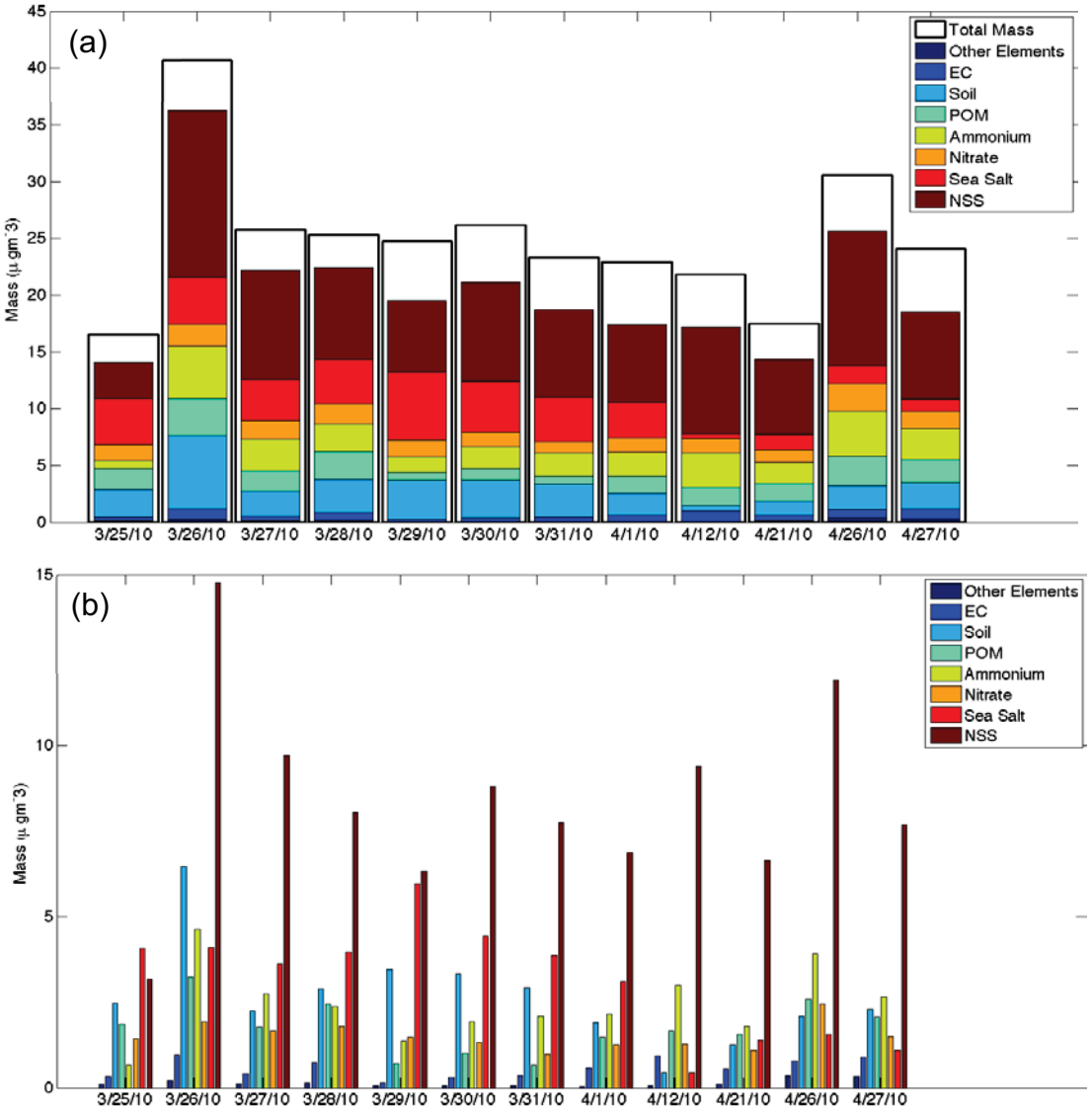

Figure 3 (a) Relative mass of chemical species derived from IMPROVE data for the period analyzed, the black outline is the total mass as measured by the weight of the filter. Our reconstructions account for ~75% of the total weight of the filter depending on the sample. (b) Same as (a) but shown to elucidate individual quantities and trends in the constituents. See text for details.

Table 3 Chemical Components and Test Parameters

Chemical Component	Conversion Factor	IOR[1] Dataset	IOR (550 nm)	Density (ρ) gcm^{-3}
Elemental carbon	Total elemental carbon	Soot (Cai, 2011)	1.96+0.66	0.5[2]
Particulate organic matter (POM)	1.6*total organic carbon [3]	Organic matter (Schkolnik et al. 2007)	1.4-0i	1.2[4,8]
Soil	2.2Al + 2.49Si + 1.63Ca + 2.42Fe + 1.94Ti [3]	Mineral dust (Patterson 1981)	1.56+0.0056	2.5[5]
Sea salt	1.8 Cl- [3]	Shettle and Fenn, 1979	1.35+2.9E-09	2.1675[6]
Non-sea salt sulphate (NSS)	Sulphate-(0.246*soluble sodium) [7]	Ammonium Sulphate[8] (Toon et al. 1976)	1.53+1.0E-07	1.769[9]
Nitrates	Nitrate*1	Ammonium Nitrate[10]	1.55+1.0E-09	1.725[11]
Other elements (IMPROVE elemental data)	As, Cd, Co, Cr, Cu, Ni, V, Br, Mm, Pb, Rb, Se, Sr, Zn	N/A[12]	N/A[12]	N/A[12]

[1] Index of Refraction
[2] Gysel et al. (2011)
[3] From Watson (2002);[Note the 1.6 multiplier for POM is in the range used by IMPROVE (1.4-1.8)]
[4] Turpin B.J. and H.-J. Lim, (2001)
[5] Representative density value based on range presented in Kandler et al. (2007).
[6] Fan and Toon (2010)
[7] Sillanpää (2006);
[8] Ammonium sulphate represents combined masses from NSS and ammonium
[9] Cai (2011)
[10] Software from Andrew Lacis (from http://gacp.giss.nasa.gov/datasets/, last visited on 23 January 2012) based on Toon et al. (1976), Gosse et al. (1997), and Tang (1996).
[11] Lloyd et al. (2009)
[12] Not applicable - not included in model analysis

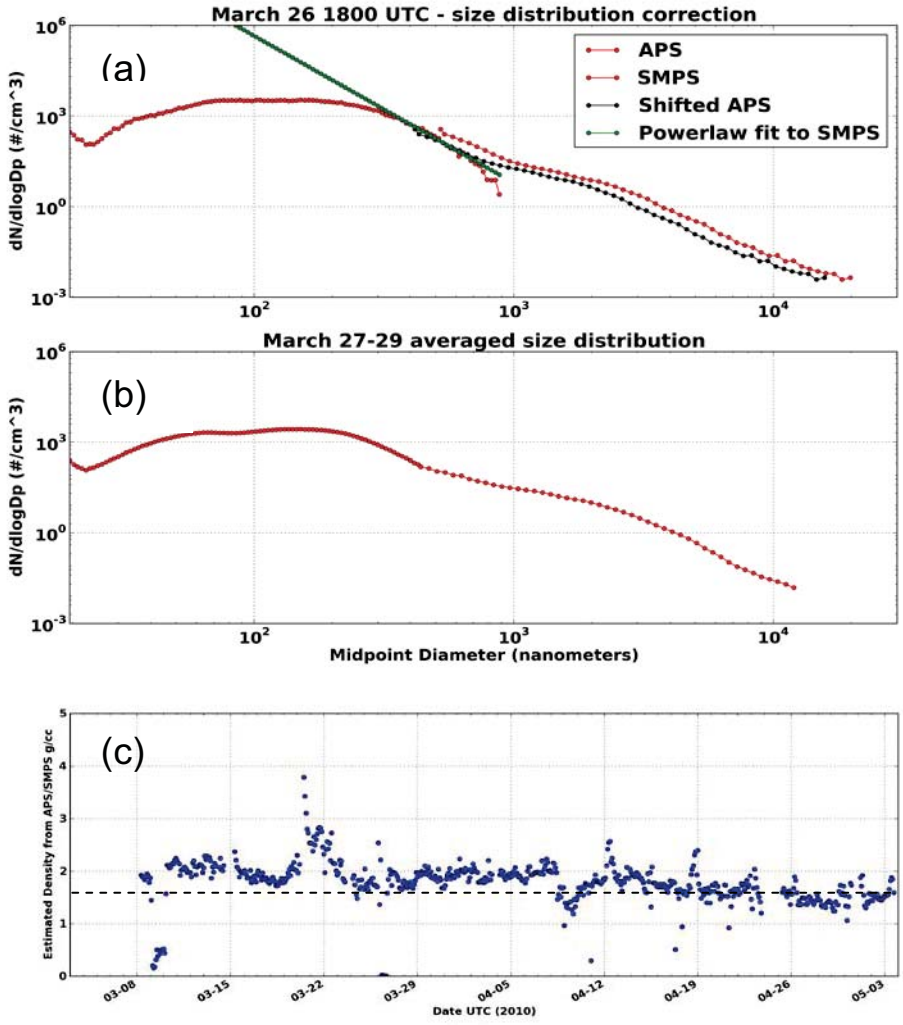

Figure 4 (a) Illustration of fitting process following the methodology of Khlystov et al. 2004 for combined SMPS and APS particle size spectra on 26 March 2010 during the 7-SEAS/Dongsha experiment. (b) Averaged size spectra from combined distribution from measurements during 27-29 March 2010 and (c) estimated particle densities with average value depicted by the dotted line. See text for details.

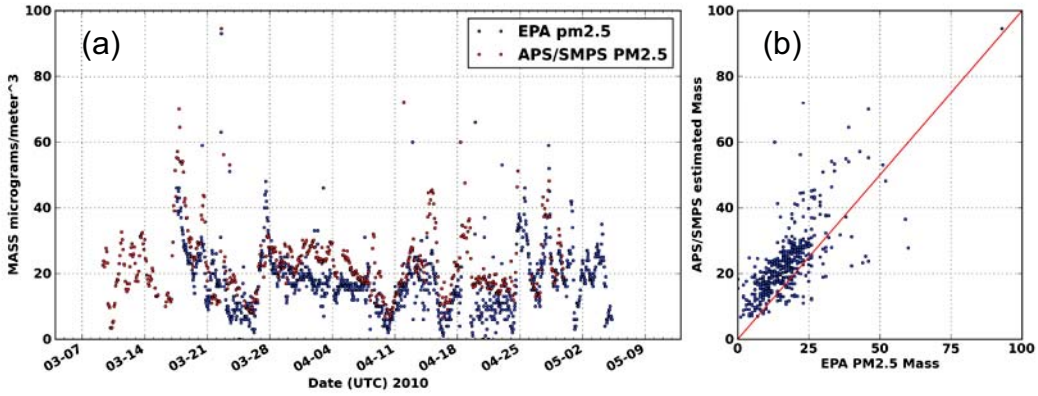

Figure 5 (a) Time series comparison of T-EPA's TEOM $PM_{2.5}$ to APS-SMPS $PM_{2.5}$ mass using the assumed bulk density for this study (b) scatterplot of the same variables with 1:1 line shown in red.

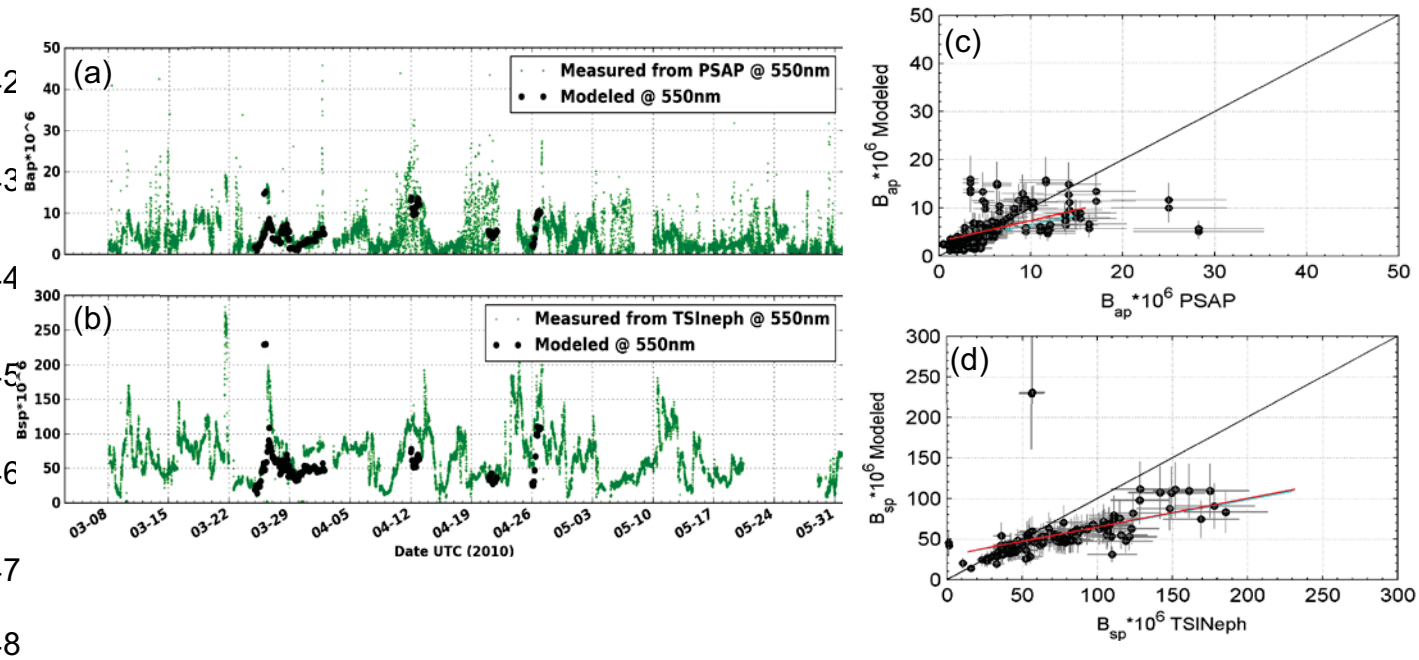

Figure 6 Time series comparisons between modeled and measured absorption coefficients (a) and scattering coefficients (b). Data in green/black are the measured/modeled coefficients, respectively. Scatter plots of absorption coefficients (c) and scattering coefficients (d). Also shown are the corresponding error bars for scattering (15%), absorption (25%), and model (30%), along with the 1:1 lines (black) and linear fits (red). All optical coefficients are in units of Mm^{-1}. See text for details.